Critical Binder cumulant and universality: Fortuin-Kasteleyn clusters and order-parameter fluctuations

Anastasios Malakis,[1] Nikolaos G. Fytas,[2] and Gül Gülpinar[3]

[1]*Department of Physics, Section of Solid State Physics, University of Athens, Panepistimiopolis, GR 15784 Zografos, Athens, Greece*

[2]*Applied Mathematics Research Centre, Coventry University, Coventry CV1 5FB, United Kingdom*

[3]*Department of Physics, Dokuz Eylül University, Buca 35160, Izmir, Turkey*

(Received 17 October 2013; revised manuscript received 19 December 2013; published 2 April 2014)

We investigate the dependence of the critical Binder cumulant of the magnetization and the largest Fortuin-Kasteleyn cluster on the boundary conditions and aspect ratio of the underlying square Ising lattices. By means of the Swendsen-Wang algorithm, we generate numerical data for large system sizes and we perform a detailed finite-size scaling analysis for several values of the aspect ratio r, for both periodic and free boundary conditions. We estimate the universal probability density functions of the largest Fortuin-Kasteleyn cluster and we compare it to those of the magnetization at criticality. It is shown that these probability density functions follow similar scaling laws, and it is found that the values of the critical Binder cumulant of the largest Fortuin-Kasteleyn cluster are upper bounds to the values of the respective order-parameter's cumulant, with a splitting behavior for large values of the aspect ratio. We also investigate the dependence of the amplitudes of the magnetization and the largest Fortuin-Kasteleyn cluster on the aspect ratio and boundary conditions. We find that the associated exponents, describing the aspect-ratio dependencies, are different for the magnetization and the largest Fortuin-Kasteleyn cluster, but in each case are independent of boundary conditions.

DOI: 10.1103/PhysRevE.89.042103 PACS number(s): 64.60.Cn, 75.10.Hk, 05.10.Ln

I. INTRODUCTION

According to the universality hypothesis [1–3], all critical systems with the same dimensionality, the same symmetry of the order parameter, and the same range of interactions are expected to share the same set of critical exponents. For the two-dimensional (2D) Ising model (square and some other lattices), all critical exponents are known exactly [4–7]. These exponents are expected to be obeyed by the Ising model on all 2D lattices and also by all other models, which according to the hypothesis are expected to belong in the same universality class. Furthermore, there is strong evidence that, in addition to critical exponents, certain critical-point ratios are universal [8–10] and of particular interest is the value of the critical Binder cumulant of the order parameter, discussed also in the present work.

The fourth-order cumulant of some thermodynamic parameter Q of a finite lattice system, known as the Binder cumulant, is defined as [8]

$$U_Q(T,L) = 1 - \frac{\langle Q^4\rangle_L}{3\langle Q^2\rangle_L^2}, \tag{1}$$

with L the linear lattice size. The critical value of the Binder cumulant of the order parameter of an Ising system is then

$$U_M^* = \lim_{L\to\infty} U_M(T = T_c, L), \tag{2}$$

with M the magnetization

$$M = (1/N)\sum_{i=1}^{N}\sigma_i, \tag{3}$$

σ_i the spin variable, and N the number of lattice sites. This parameter is a measure of the deviation of the universal probability density function from a Gaussian function. It is well known that the characteristic behavior of U_M [8,11] near criticality provides a traditional route to obtain transition temperatures (from the intersection of the cumulants of systems with different sizes) and may also be used to extract the critical exponent ν of the correlation length [8–10]. Its critical value, U_M^*, was originally believed to fully characterize a given universality class. As discussed by various authors, the same value seems to be shared by several 2D models, such as the *XY* models with an easy axis, the nearest-neighbor spin-1 Ising model, and the isotropic nearest-neighbor Ising-like models, including also the nearest-neighbor "border ϕ^4 model" with softened spins [12–18]. It appears also to be independent of the lattice details, such as the lattice structure [19,20]. However, this "universality" applies only in a limited sense. The value of U_M^* does depend on the boundary conditions [8,11], the shape of the system [13,17,21–25], as well as on the symmetry of the interactions [19].

An accurate estimation of critical-point ratios for the ferromagnetic Ising model on the square and triangular lattices has been provided via the transfer-matrix technique [13]. In this paper, Kamieniarz and Blöte estimated U_M^* as a function of the aspect ratio r (see discussion below for the definition of r), reporting, in particular for the square Ising model with periodic boundary conditions and $r = 1$, the value $U_M^* = 0.61069\ldots$. The influence of the anisotropic interactions on the critical Binder cumulant was studied, analytically, by Dohm and Chen [24,25] and, numerically, by Selke and Shchur [21,22], indicating that U_M^* depends continuously on the anisotropy, in the case of periodic boundary conditions and $r = 1$. Furthermore, Kastening [26] obtained a renormalization-group quantitative description of the anisotropy dependence of U_M^*.

In the present paper, we investigate certain aspects of the critical Binder cumulant and, in particular, its dependence on the boundary conditions and the relevant aspect ratio of the lattice. We concentrate our interest on numerical observations illustrating parallel behavior to that of the critical Binder cumulant of the largest Fortuin-Kasteleyn cluster (LFKC). The rest of the paper is organized as follows: In the next section,

we define the model and outline the numerical details. Then, in Sec. III, we present and discuss our numerical findings. Finally, we summarize our conclusions in Sec. IV.

II. MODEL AND SIMULATION DETAILS

Let the size of the LFKC be denoted by $\mathcal{S}_{\mathrm{LFKC}}$ and let us define, in analogy to the magnetization, $l_\infty = \mathcal{S}_{\mathrm{LFKC}}/N$. Then, the relevant critical Binder cumulant may be denoted as $U_{l_\infty}^*$. To be concrete, we consider the square Ising model in zero field, with the standard Hamiltonian

$$\mathcal{H} = -J \sum_{\langle ij \rangle} \sigma_i \sigma_j, \tag{4}$$

where the spin variables σ_i take the Ising values ± 1 and $\langle ij \rangle$ denotes summation over all nearest-neighbor pairs of sites. For the needs of our study, we construct ferromagnetic nearest-neighbor square Ising systems with L rows and $L_1 = rL$ columns, corresponding to $N = L \times L_1 = L \times rL \equiv (L^*)^2$ sites. Furthermore, we consider several values of the aspect ratio $r = \{1,4,9,16,25,36,50,64,100\}$, and investigate both periodic (PBC) and free boundary conditions (FBC). As our numerical vehicle, we implement the Swendsen-Wang algorithm [27–30], and we identify clusters by the Hoshen-Kopelman procedure [29,31].

The comprehensive Monte Carlo study of De Meo *et al.* [32] presented a review of the connections of Fortuin and Kasteleyn's work [33] to the Swendsen-Wang algorithm and a review of the relevant literature. In this study, the authors investigated the scaling properties of the cluster size distribution and provided a numerical verification of the theoretical results given by Hu [34]. In particular, they showed that the relevant bond-correlated percolation model has the Ising critical temperature and critical exponents. Thus, it is generally assumed, that the LFKC corresponds to the magnetization, but the distribution functions and, accordingly, the Binder cumulants are quite different.

We concentrate on the dependency of the critical Binder cumulants, U_M^* and $U_{l_\infty}^*$, on the boundary conditions and the aspect ratio and compare our results with previous work when available [13,19,35]. We also illustrate and compare the corresponding probability density functions (pdfs), observing their evolution as a function of the aspect ratio. For PBC and $r = 4$, a pronounced double-peak structure is observed in the pdf of LFKC, and we give for this a geometrical explanation, involving the probability that the LFKC percolates along both (short and long) directions of the lattice simultaneously. Finally, we discuss the critical-exponent equivalence [32,34] and the scaling properties of $Q = |M|$ and $Q = l_\infty$, for both PBC and FBC. In particular, we estimate the amplitudes A_Q of the power law $\langle Q \rangle = A_Q L^{-\beta/\nu}$ for all values of the aspect ratio considered. It is shown that these amplitudes follow a power law with r, and the corresponding exponents are determined. This analysis is related to the interesting superscaling concepts reported by Watanabe *et al.* [36] in their study of percolation on rectangular domains, as will be further discussed below.

The square Ising systems under study were simulated only at the exact critical temperature $k_B T_c/J = 2.2691853\ldots$. In our numerical approach, we define a Swendsen-Wang Monte Carlo step to consist of 10–20 (depending on L^*) Swendsen-Wang moves, in which all Fortuin-Kasteleyn clusters attempt to flip with probability 1/2 [27,28]. A number of Swendsen-Wang Monte Carlo steps, denoted as n_{eq}, is used for equilibration and a large number of such steps, denoted as n_{rec}, is used for the recording of the data related to the Fortuin-Kasteleyn cluster decomposition. Typical values of the parameters n_{eq} and n_{rec}, used in our simulations, are $n_{\mathrm{eq}} = 1600$ and $n_{\mathrm{rec}} = 64\,000$ for $L^* = 20$, whereas $n_{\mathrm{eq}} = 7200$ and $n_{\mathrm{rec}} = 115\,200$ for $L^* = 120$. In each case, we used 10 independent runs, restarted from new random spin configurations. The statistical errors of the corresponding data were set equal to 3 standard deviations of the 10 independent runs.

In order to achieve good accuracy in the estimation of the above-mentioned amplitudes, via an extrapolation finite-size scaling scheme, the above-described simulations were carried out for all values of aspect ratio r. In all cases, approximately the range $L^* = 20$–120 was covered by 8–10 different widths L, and for $r = 1$ and $r = 4$, we also simulated systems with linear sizes $L = 160$ and 200.

III. NUMERICAL RESULTS AND DISCUSSION

All of our estimates for the critical Binder cumulants are given in Table I, together with the existing ones from the corresponding literature. In Fig. 1, we illustrate the finite-size behavior of the critical cumulants for a selected set of the cases (as indicated on the panel), and the rather smooth linear extrapolation, which provides us with the limiting values of the critical Binder cumulants. The values listed in Table I were obtained by applying the expected leading correction term $aL^{-1.75}$ [13]. Note that, in almost all cases, these values and the ones obtained by a linear extrapolation

TABLE I. Critical Binder cumulants of the order parameter and the LFKC for PBC and FBC and several values of the aspect ratio r. The numbers in parentheses denote errors.

BC	r	U_M^* [a]	U_M^*	$U_{l_\infty}^*$
PBC	1	0.61069 . . . [13]	0.61067(24)	0.6167(2)
PBC	4	0.48723 . . . [13]	0.48697(36)	0.4995(5)
PBC	9	0.27054 . . . [13]	0.2713(10)	0.3880(8)
PBC	16		0.1539(6)	0.4317(10)
PBC	25		0.0984(10)	0.4760(6)
PBC	36		0.0685(10)	0.5044(10)
PBC	50	0.04920 . . . [13]	0.0493(5)	0.5258(15)
PBC	64		0.0375(12)	0.5385(8)
PBC	100	0.02454 . . . [13]	0.0242(20)	0.5585(10)
FBC	1	0.396(2) [19]	0.3969(6)	0.4370(10)
FBC	4		0.2365(15)	0.3898(10)
FBC	9		0.1188(12)	0.4394(80)
FBC	16		0.0680(5)	0.4860(40)
FBC	25		0.0452(14)	0.5160(20)
FBC	36		0.0330(6)	0.5365(5)
FBC	50		0.0214(10)	0.5533(12)
FBC	64		0.0178(15)	0.5631(15)
FBC	100		0.0123(10)	0.5790(10)

[a]Best estimates from the literature.

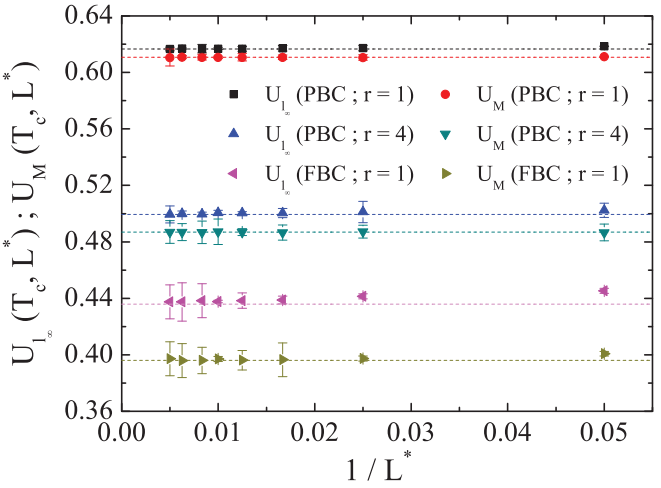

FIG. 1. (Color online) Illustration of the finite-size behavior of critical Binder cumulants for the magnetization U_M^* and the LFKC $U_{l_\infty}^*$. Cases of PBC with $r = 1$ and $r = 4$ and FBC with $r = 1$ are illustrated. The dashed lines are the extrapolated limits.

agree within error bars. From the table, one can observe a very good agreement with previous estimates regarding the magnetization's critical Binder cumulants and the estimates of the present study. The critical Binder cumulants of the LFKC ($U_{l_\infty}^*$) are found, in all cases, to be upper bounds to the values of the critical Binder cumulants of the order parameter. The smallest difference between the two cumulants corresponds to the case of PBC with $r = 1$ and this difference is enhanced as the order-parameter cumulant deviates from the value 2/3, approaching the limiting (Gaussian) value 0, as $r \to \infty$.

This strong splitting behavior is presented in Fig. 2, which gives a full illustration of the dependence of critical Binder cumulants for magnetization and the LFKC on the aspect ratio for both cases of boundary conditions considered. Several interesting conclusions can be drawn from this figure. First, as should be expected, and shown by Kamieniarz and Blöte [13]

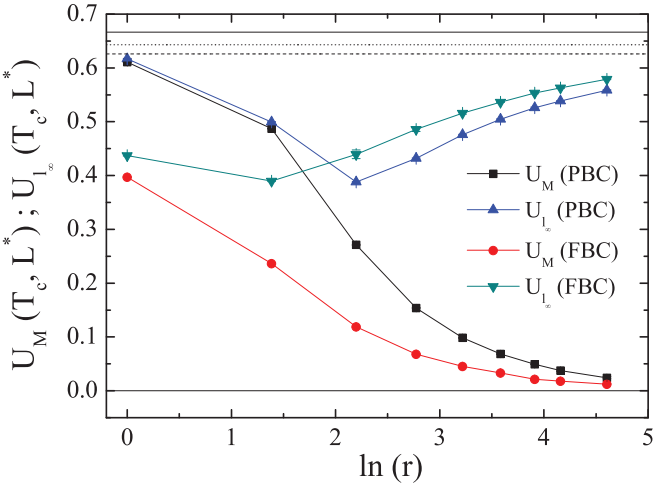

FIG. 2. (Color online) Dependence of critical Binder cumulants U_M^* and $U_{l_\infty}^*$ on the logarithm of the aspect ratio $\ln(r)$ for PBC and FBC.

for PBC, the limiting magnetization cumulants U_M^* agree with the Gaussian value 0, describing linear systems, as $r \to \infty$ for both PBC and FBC. For large r, $U_M^*(r)$ becomes linear in r^{-1}, and, as pointed out by Kamieniarz and Blöte [13], the product $A_U(r) = rU_M(r)$ approaches exponentially fast the universal amplitude $A_U = \lim_{r\to\infty}[U_M^*(r)r]$. The estimates for this universal amplitude of the transfer-matrix technique in Ref. [13] agree to ∼5 significant figures with the value $A_U = 2.46044(2)$, obtained from conformal invariance [35]. The statistical Monte Carlo errors permit here a moderately accurate estimate of the order of $A_U = 2.466(7)$, as can be seen by a linear fit of the $r = 16$–100 data of Table I. For FBC, $U_M^*(r)$ becomes also linear in r^{-1}, and the corresponding fit, in the range $r = 16$–100, provides the estimate $A_U = 1.055(26)$.

The cumulant $U_{l_\infty}^*$ of the LFKC shows a nonmonotonic behavior approaching, finally, as $r \to \infty$, a nontrivial value different to 2/3 (describing the ordered phase). To estimate the limiting behavior, we assume the law $U_{l_\infty}^*(r) = U_{l_\infty}^*(\infty) - Br^{-x}$. Fitting the $r = 16$–100 or the $r = 25$–100 data of Table I, we find quite stable estimates. For the $r = 25$–100 range, this estimation scheme gives $U_{l_\infty}^*(r) = 0.626(4) - 0.96(4)r^{-0.57(2)}$ for PBC, and $U_{l_\infty}^*(r) = 0.643(10) - 0.63(7)r^{-0.50(6)}$ for FBC. Although, even for $r = 100$, the values of the cumulants deviate significantly from their limiting values, the exponents x agree with the value 0.5 within error bars and appear to be independent of the boundary conditions. Thus, the exponents controlling the limiting r behavior are different for $U_M^*(r)$ and $U_{l_\infty}^*(r)$, but are independent of the boundary conditions. Note that the above limiting values are indicated by the dashed (PBC) and dotted (FBC) lines in the panel of Fig. 2 together with the full line corresponding to the value 2/3. In the limit $r \to \infty$, cumulant universality between PBC and FBC is reflected in the exponents, and the role of the boundary conditions appears to diminish in that limit. As noted above, for moderate values of the aspect ratio, both U_M^* and $U_{l_\infty}^*$ have a strong dependence on the boundary conditions. This nonmonotonic behavior, and the smooth final approach in the limit $r \to \infty$, are reflections of the evolution features of the corresponding pdfs, which are further illustrated below.

Figure 3 illustrates the scaling of the order-parameter pdfs, while Fig. 4 illustrates the scaling of the relevant functions of the LFKC for the cases with PBC and FBC, for which their Binder's cumulant finite-size behavior is illustrated in Fig. 1. The scaled distributions have been constructed by using as scaling variables the $x = Q/\sqrt{\langle Q^2\rangle}$ [8,23,37–40], with $Q = |M|$ or $Q = l_\infty$. In the scaling limit (system size going to infinity), these functions are expected to be universal and characterize the given universality class [8,37]. The scaled density functions are then obtained from $p(x)dx = p_Q(Q)dQ$, i.e., $p(x) = p_Q(Q)\sqrt{\langle Q^2\rangle}$, and also a smoothing process of the fluctuations has been applied. The pronounced double-peak structure for PBC and $r = 4$, the left shoulders for PBC and $r = 1$ observed in Fig. 4, and also the nonmonotonic behavior of the critical cumulant of the LFKC of Fig. 2 are interesting findings reflecting geometrical features of the present bond-correlated percolation model. A brief qualitative description of these features is attempted below, observing the variation of certain percolation probabilities with the aspect ratio (r).

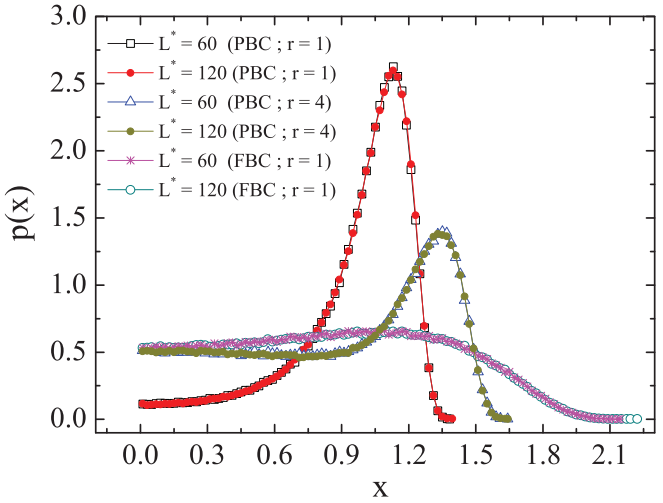

FIG. 3. (Color online) Scaled pdfs of the magnetization, $x = |M|/\sqrt{\langle M^2 \rangle}$, for (i) PBC with $r = 1$ and $r = 4$ and (ii) FBC with $r = 1$. Sizes $L^* = 60$ and $L^* = 120$ are illustrated.

Throughout the years, different percolation probabilities have appeared in the literature [41–43], using different terms such as spanning probability [41], crossing probability [43], or existence probability [36,42]. It is well known that above the percolation threshold, there exists an infinite cluster with probability one [44], while exactly at the percolation threshold, the "crossing probabilities" need not be one and their study is an important topic with many and famous contributions, such as Cardy's exact result [43] on the square lattice with FBC. These critical probabilities depend on the boundary conditions and the aspect ratio [36,45]. For the square systems considered here, with L rows and $L_1 = rL$ columns, we define p_{short} to be the probability that the LFKC percolates only in the short direction, visiting every row of the lattice (that is, having at least one point in every row). Respectively, the corresponding probability that the LFKC percolates only in the long direction, visiting all columns, will be denoted by p_{long},

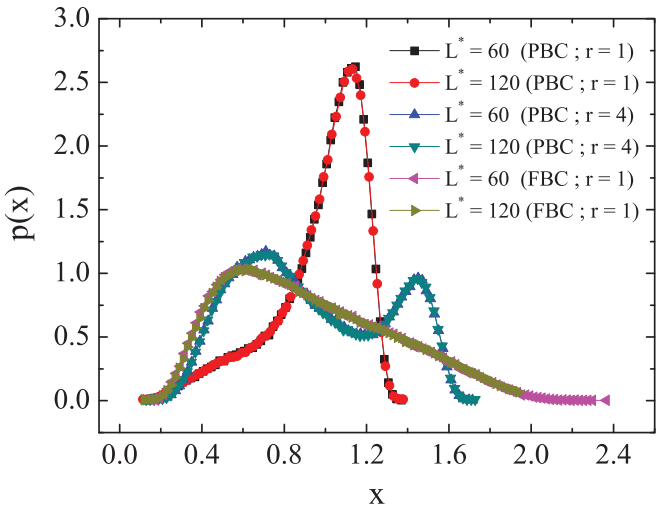

FIG. 4. (Color online) Scaled probability pdfs of the LFKC, $x = l_\infty/\sqrt{\langle l_\infty^2 \rangle}$, corresponding to the cases of Fig. 3.

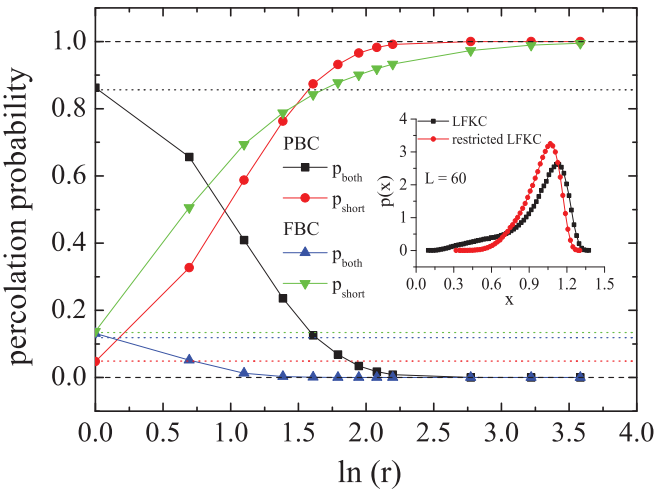

FIG. 5. (Color online) Percolation probabilities p_{both} and p_{short} with respect to $\ln(r)$. Dashed lines indicate the $r = 1$ values in the thermodynamic limit (see discussion in the text), and the expected large-r behavior. The crossover behavior for the PBC is associated with the appearance of the double-peak structure in Fig. 4. In the inset, we compare the $r = 1$ shoulderlike behavior in Fig. 4 with a restricted pdf describing only the LFKC that percolates simultaneously in both directions.

and the probability of simultaneously percolating in both the short and long directions will be denoted by p_{both}. We may note here that for the present bond-correlated LFKC percolation, at the critical point, the sum $p_{\text{span}} = p_{\text{both}} + p_{\text{long}} + p_{\text{short}}$ (spanning probability in some direction) will also depend on the boundary conditions and the aspect ratio and need not be one. The behavior of p_{both} and p_{short} as a function of r is illustrated in Fig. 5 for both PBC and FBC. Clearly, a strong variation with respect to the aspect ratio r is observed. To construct Fig. 5, we have used systems with approximately 3600 lattice sites. For instance, for $r = 2$, lattices of 42×84 with 3528 lattice points were used, while for $r = 36$, lattices of 10×360 with 3600 lattice points were used. Additionally, for $r = 1$, we carried out a brief finite-size scaling analysis using data in the range $L = 30$–100. The resulting limiting values are indicated with the dashed lines in Fig. 5 and demonstrate that the finite-size behavior in the main panel, using systems with 3600 lattice sites, is already a genuine representation of the behavior in the thermodynamic limit. As can be seen, for moderate values of r and PBC, the LFKC percolates with significant probabilities in both directions of the square lattice, giving rise to the double-peak structure. Then, as r grows, the probability for percolation along the width of the rectangular lattices increases substantially, whereas it declines along the length direction, leading to the evaporation of the right peak. The crossing of the probabilities for PBC, in the main panel of Fig. 5, gives a clear explanation of the observed double-peak structure, while the absence of such a structure in the case of FBC is due to the very early and large separation of the corresponding probabilities. The presence of the left shoulders for PBC and $r = 1$, in the pdf of the LFKC shown in Fig. 4, may also be explained by the existence of a nonvanishing contribution of LFKC percolating only in one lattice direction. This is illustrated in the inset of Fig. 5, where we compare this

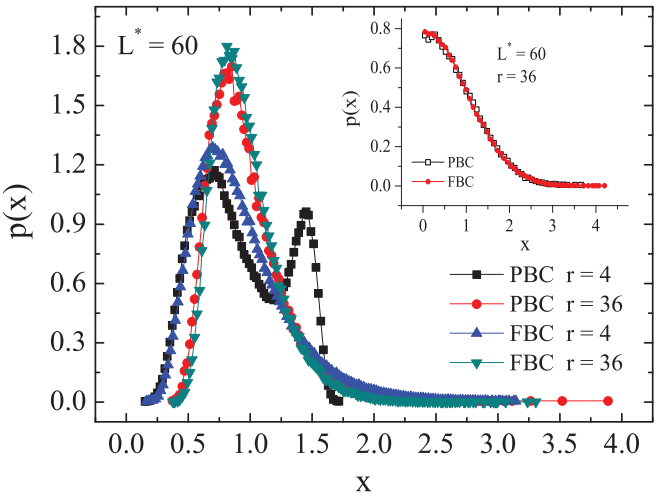

FIG. 6. (Color online) Main panel: Scaled pdfs of the LFKC, $x = l_\infty/\sqrt{\langle l_\infty^2\rangle}$, for PBC and FBC. Illustration of striking differences for $r = 4$ and approach to the same universal pdf as r increases ($r = 36$). Inset: Illustration of the similarity of the magnetization's pdfs, $x = |M|/\sqrt{\langle M^2\rangle}$, for large r ($r = 36$).

shoulderlike behavior to a restricted pdf describing only the LFKC that percolates simultaneously in both directions.

Subsequently, Fig. 6 clarifies in the main panel the diversity in the shape of the pdfs of the LFKC for the cases with PBC and FBC for moderate aspect-ratio values and the similarity in the shape for larger values ($r = 36$). The inset of the same figure points out the similarity in the shape of the magnetization pdfs for $r = 36$.

Differences in the shapes of the universal pdfs of the magnetization and the LFKC should be expected from the theoretical arguments of Hu [34] and the Monte Carlo study of De Meo *et al.* [32]. As shown numerically in Ref. [32], below T_c the magnetization susceptibility differs from the corresponding percolation susceptibility. Thus, the above illustrations reveal these differences at T_c, but also show a variability in the behavior for moderate values of the aspect ratio. The illustrations in Fig. 7 give a sketch of the evolution of both pdfs, as we increase the aspect ratio from $r = 1$ to $r = 16$ in the case of PBC. From Fig. 7(a), for the case $r = 1$, we observe a small but noticeable difference in the left tails, which is, however, enough to produce the small difference of the cumulant values in Table I. The double-peak structure of the pdf of the LFKC for $r = 4$, in Fig. 7(b), is associated to the pronounced left tail in the pdfs of the magnetization. For larger values of the aspect ratio [see Figs. 7(c) and 7(d)], the pdfs of the LFKC tend to the shape illustrated in the main panel of Fig. 6 for $r = 36$, and the corresponding pdfs of the magnetization to the one illustrated in the inset of Fig. 6 for $r = 36$. Now, according to Refs. [32,34], the behavior of $\langle Q\rangle$, with $Q = |M|$ or $Q = l_\infty$, should be expected to be described by the same power law of the form $\langle Q\rangle = AL^{-\beta/\nu}$, with the critical exponent having the 2D Ising value $\beta/\nu = 0.125$. Thus, as we vary the aspect ratio, the corresponding leading amplitudes, $A_{|M|}$ and A_{l_∞}, decrease and describe the asymptotic shifts to smaller mean values. These shifts are considerable and are responsible for the development of a Gaussian-like shape in

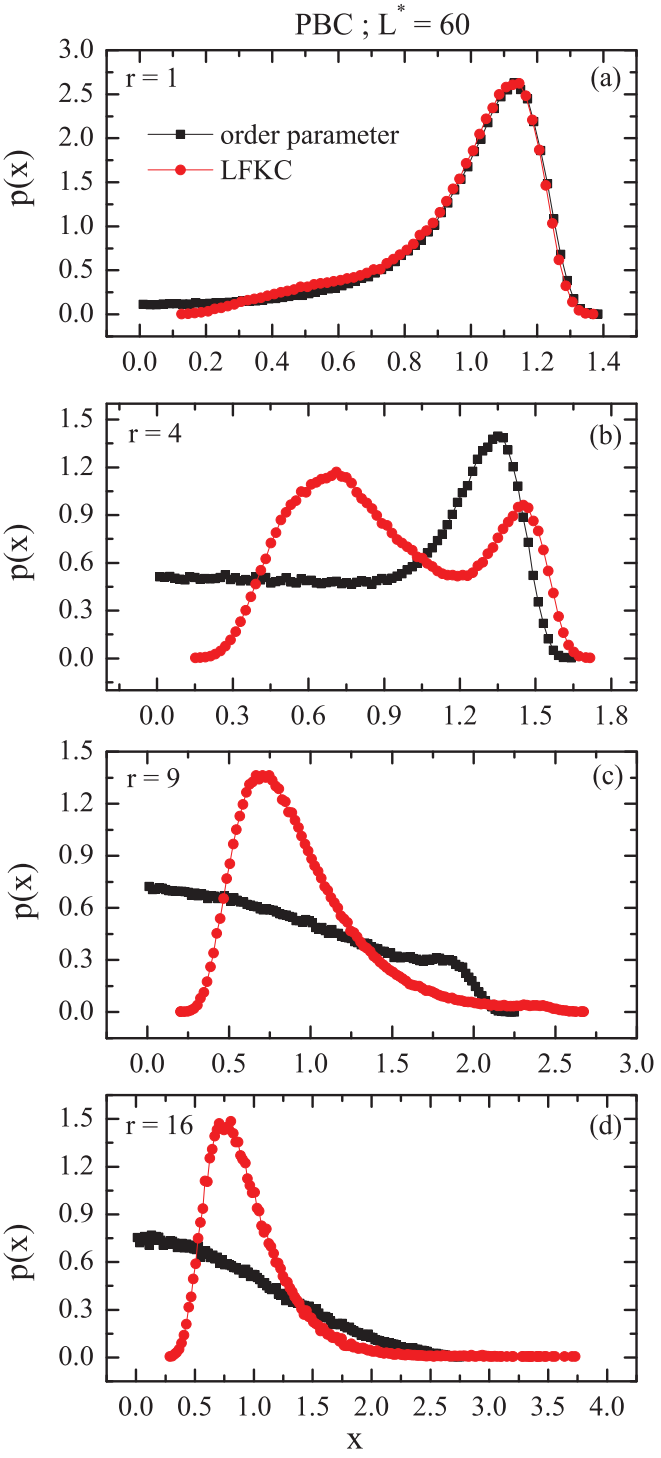

FIG. 7. (Color online) Scaled pdfs of the magnetization, $x = |M|/\sqrt{\langle M^2\rangle}$, and the LFKC, $x = l_\infty/\sqrt{\langle l_\infty^2\rangle}$, for PBC as we vary the aspect ratio in the window $r = 1$–16. This figure elucidates the similarity among the two functions for $r = 1$, but also highlights their striking differences with increasing r.

the small M behavior of the pdfs of the magnetization, as also illustrated in the inset of Fig. 6 for $r = 36$.

From the shape of the pdfs of the LFKC in Fig. 4, and also from the comparative plot of Fig. 7, we observe that larger fluctuations (widths) of the LFKC enhance, in all cases, the left

tail of the magnetization's pdf, since smaller Fortuin-Kasteleyn clusters favor the mixing of positive and negative spin clusters. However, for large values of the aspect ratio, the pronounced $M = 0$ behavior of the universal pdfs is mainly due to the shifts of the density functions of the LFKC, discussed above. Comparing their shapes, i.e., Figs. 3 and 4, we can appreciate this evolution for the case of FBC with $r = 1$ and also for the case with PBC and $r = 4$. The large fluctuations of the LFKC and their shifts to smaller mean values induce similar behavior on the statistically significant part of the Fortuin-Kasteleyn clusters, which contribute and enhance the small M behavior of the order-parameter pdf.

Let us now consider the scaling properties of $|M|$ and l_∞, and the critical-exponent equivalence [32,34]. In order to observe quantitatively the scaling properties of the above distributions, we attempted to apply to our data a simple power law, $\langle Q \rangle = A_Q L^{-\beta/\nu}$, and furthermore other expansions, including algebraic powers, but also logarithmic terms, $\langle Q \rangle = A_Q L^{-\beta/\nu}[1 + B \ln(L)/L + C/L + \cdots]$. For PBC and almost all values of r, the simple power law produced stable estimates with effective exponents converging to the 2D Ising value $\beta/\nu = 0.125$. Furthermore, by fixing the exponent to the above expected value, and varying the width range $L = (L_{\min} - L_{\max})$, we obtained smoothly behaving effective values for the corresponding amplitudes A_Q. Employing a linear extrapolation in $1/L_{\min}$ to the above effective values, we found very accurate estimates for the amplitudes in the thermodynamic limit. The same procedure was also followed using the simplest correction form $\langle Q \rangle = A_Q L^{-\beta/\nu}(1 + B/L)$, giving final estimates which are the same, within error bars, as those obtained by the simple power law. For the case of FBC, the fitting attempts to the simple power law produce, in general, overestimated values of the exponent, and by fixing $\beta/\nu = 0.125$, the resulting effective values of amplitudes A_Q deviate significantly from their asymptotic values. However, the fitting attempts to the form $\langle Q \rangle = A_Q L^{-\beta/\nu}(1 + B/L)$ gave a smooth behavior of effective amplitudes with small deviations of their asymptotic values, allowing an accurate estimation of the amplitudes.

In particular, for the case of PBC with $r = 1$, we found, by applying a simple power law, $\beta/\nu = 0.1248(4)$ from the magnetization data and $\beta/\nu = 0.1249(2)$ from the l_∞ data, with corresponding amplitudes $A_{|M|} = 1.008(2)$ and $A_{l_\infty} = 1.007(2)$. However, this was an exceptionally good case, while for FBC with $r = 1$, the simple power law, when applied in the range $L = 20$–96, produces the results $\langle |M| \rangle = 0.581(5) L^{-0.146(2)}$ and $\langle l_\infty \rangle = 0.556(4) L^{-0.145(2)}$. Moving to larger values of $L_{\min}$, upon using the range $L = 60$–96, we found $\langle |M| \rangle = 0.559(5) L^{-0.137(2)}$ and $\langle l_\infty \rangle = 0.541(3) L^{-0.139(1)}$. Thus, even the simple power law improves the estimation by increasing $L_{\min}$. However, the fitting attempts using the correction term are now most effective, giving, in the range $L = 20$–96, $\langle |M| \rangle = 0.520(5) L^{-0.124(2)}[1 + 1.07(9)/L]$ and $\langle l_\infty \rangle = 0.504(4) L^{-0.125(2)}[1 + 0.98(7)/L]$. The sequence of effective estimates resulting from the scheme with the correction term and a fixed exponent to the expected value $\beta/\nu = 0.125$ converges smoothly to $A_{|M|} = 0.5239(4)$ and $A_{l_\infty} = 0.5031(4)$. These results indicate that the amplitudes of $\langle |M| \rangle$ and $\langle l_\infty \rangle$ are, in general, different and, in the case of FBC, the simplest correction term B/L is very effective since the effective estimates of the range $L = 20$–96 are already very close to their asymptotic values.

TABLE II. Amplitudes of the power law $\langle Q \rangle = A_Q L^{-\beta/\nu}$ obtained by the schemes detailed in the text using the data of magnetization and the LFKC.

	PBC		FBC	
r	$A_{\|M\|}$	A_{l_∞}	$A_{\|M\|}$	A_{l_∞}
1	1.008(2)	1.007(2)	0.5239(4)	0.5031(4)
4	0.7204(1)	0.7073(1)	0.3550(10)	0.3250(50)
9	0.4674(2)	0.4251(3)	0.2470(60)	0.1970(30)
16	0.3436(4)	0.2826(4)	0.1896(2)	0.1335(2)
25	0.2727(2)	0.2033(2)	0.1530(4)	0.0965(1)
36	0.2259(2)	0.1542(2)	0.1278(2)	0.0732(1)
50	0.1912(12)	0.1198(3)	0.1088(3)	0.0567(4)
64	0.1689(9)	0.0988(9)	0.0962(4)	0.0466(2)
100	0.0764(2)	0.0697(6)	0.0764(8)	0.0325(2)

The systematic application of the above-described extrapolation schemes verifies that for all aspect ratios r, the amplitude $A_{|M|}$ is higher than A_{l_∞} and, in fact, their difference grows with increasing r. This is an interesting topic related to the theoretical arguments of Hu [34] and to the superscaling concepts reported by Watanabe *et al.* in their study of percolation on rectangular domains [36]. Adapting this superscaling proposal of Ref. [36] to our study at criticality, we assume that the above amplitudes follow, for large r, a power law. This is equivalent to the proposal $\langle Q \rangle = a r^{-z} L^{-\beta/\nu}(1 + \cdots)$ and thus, for the relevant amplitudes, we associate a superscaling exponent z. Watanabe *et al.* [36] have pointed out the interest of a study of their superscaling concept to correlated percolation models [34,46], such as the present model. In order to verify these concepts, in the realm of the present study, we have carried out an accurate estimation of the amplitudes for all r considered here. Our estimates are given in Table II and the general behavior is illustrated in Fig. 8. The amplitudes of the magnetization follow closely, for large enough r, say $r \geqslant 9$, a simple power law of the form $A_{|M|}(r) = a r^{-z}$, with small corrections. Thus, for PBC, we obtain $A_{|M|}(r) = 1.361(9) r^{-0.50(2)}$, whereas for FBC, $A_{|M|}(r) = 0.762(9) r^{-0.50(2)}$. For the amplitudes A_{l_∞} of the LFKC, the deviations from the simple power law are larger. Now, a correction term of the form B/r stabilizes the behavior of the effective estimates. Thus, in the case of PBC, we find $A_{l_\infty}(r) = 3.01(10) r^{-0.816(14)}[1 - 1.71(20)/r]$, while $A_{l_\infty}(r) = 1.42(5) r^{-0.816(14)}[1 - 1.52(22)/r]$ for the case of FBC. The above asymptotic behaviors have been illustrated in Fig. 8 by drawing the corresponding lines through the estimates in the range $r \geqslant 3$. As expected (see also Ref. [36]), the power laws apply only for systems with large r.

IV. CONCLUSIONS

To summarize our conclusions, the amplitudes of $\langle |M| \rangle$ and $\langle l_\infty \rangle$ are, in general, different and depend on the boundary conditions. Their dependence on the aspect ratio r can be meaningfully described by the superscaling concepts of

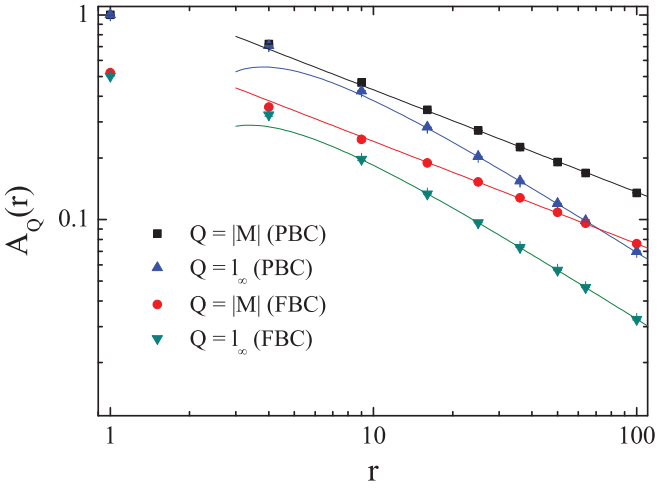

FIG. 8. (Color online) Amplitude dependence on r and illustration of the power law $A_Q(r) = ar^{-z}$ on a double logarithmic scale. The lines through the estimates in the range $r \geqslant 3$ represent only the asymptotic behaviors, as also discussed in the main text.

Ref. [36], and by estimating the corresponding exponents. These superscaling exponents (z) are certainly different for $\langle |M| \rangle$ and $\langle l_\infty \rangle$, but are independent of the boundary conditions. This universality with respect to the boundary conditions appears to be also valid, as we have shown, for the approach of the cumulants to their limiting values for large r. Our illustrations of the distribution functions allow for a better understanding of the different behaviors of the Binder cumulants and provide an interpretation showing the dominance of the fluctuations of the LFKC and the importance of their shifts for the corresponding order-parameter's universal distribution functions. Larger fluctuations of the LFKC and their shifts to smaller values induce similar behaviors on the statistically significant part of the Fortuin-Kasteleyn clusters, enhancing the small order-parameter behavior, which is mainly responsible for large deviations of the critical cumulant from the value 2/3 of the ordered phase. A straightforward future challenge emerging from the current work would be to test the above findings for different lattice geometries and higher dimensions.

The main issue of this work was to explain, by looking at the geometrical sensitivity of the LFKC upon varying the boundary conditions and the aspect ratio, the interesting behavior of critical Binder cumulants of the order parameter. As shown, these features are reflected in the distribution functions of the LFKC and it should be underlined at this point that one aspect of the fundamental achievement in the theory of equilibrium critical phenomena, i.e., the confirmation of universality and the calculation of critical exponents, has been obtained via the pdfs of the main thermodynamic variables of the system at criticality. The use of the universal character of the order-parameter pdf in describing critical properties of models in statistical mechanics has been shown to be quite valuable [8,23,37–40,47], has been extended to the study of pure and disordered magnetic systems, and is of current interest (for a recent review and update on the topic, see Ref. [47]).

ACKNOWLEDGMENTS

The authors would like to thank Professor Walter Selke for a careful reading of the manuscript and useful comments, as well as Niklas Fricke for useful correspondence, pointing out that the fluctuations of the order parameter are probably dominated by the size of the largest Fortuin-Kasteleyn cluster.

[1] M. E. Fisher, Phys. Rev. Lett. **16**, 11 (1966).
[2] R. B. Griffiths, Phys. Rev. Lett. **24**, 1479 (1970).
[3] L. P. Kadanoff, Phys. B **2**, 263 (1966).
[4] L. Onsager, Phys. Rev. **65**, 117 (1944).
[5] B. Kaufman, Phys. Rev. **76**, 1232 (1949).
[6] C. N. Yang, Phys. Rev. **85**, 808 (1952).
[7] R. J. Baxter, *Exactly Solved Models in Statistical Mechanics* (Academic, London, 1982).
[8] K. Binder, Z. Phys. B: Condens. Matter **43**, 119 (1981); Phys. Rev. Lett. **47**, 693 (1981).
[9] V. Privman and M. E. Fisher, Phys. Rev. B **30**, 322 (1984).
[10] H. W. Blöte and M. P. Nightingale, Physica A **134**, 274 (1985).
[11] K. Binder and D. W. Heermann, *Monte Carlo Simulation in Statistical Physics* (Springer-Verlag, Berlin, 1988).
[12] D. Nicolaides and A. D. Bruce, J. Phys. A: Math. Gen. **21**, 233 (1988).
[13] G. Kamieniarz and H. W. J. Blöte, J. Phys. A: Math. Gen. **26**, 201 (1993).
[14] W. Rżysko, A. Patrykiejew, and K. Binder, Phys. Rev. B **72**, 165416 (2005).
[15] M. Holtschneider, W. Selke, and R. Leidl, Phys. Rev. B **72**, 064443 (2005).
[16] G. Schmid, S. Todo, M. Troyer, and A. Dorneich, Phys. Rev. Lett. **88**, 167208 (2002).
[17] W. Janke, M. Katoot, and R. Villanova, Phys. Rev. B **49**, 9644 (1994).
[18] C. Holm, W. Janke, T. Matsui, and K. Sakakibara, Physica A **246**, 633 (1997).
[19] W. Selke, Eur. Phys. J. B **51**, 223 (2006).
[20] W. Selke, J. Stat. Mech.: Theory Exp. (2007) P04008.
[21] W. Selke and L. N. Shchur, J. Phys. A: Math. Gen. **38**, L739 (2005).
[22] W. Selke and L. N. Shchur, Phys. Rev. E **80**, 042104 (2009).
[23] R. Hilfer, B. Biswal, H. G. Mattutis, and W. Janke, Phys. Rev. E **68**, 046123 (2003).
[24] X. S. Chen and V. Dohm, Phys. Rev. E **70**, 056136 (2004).
[25] V. Dohm, Phys. Rev. E **77**, 061128 (2008).
[26] B. Kastening, Phys. Rev. E **87**, 044101 (2013).
[27] R. H. Swendsen and J. S. Wang, Phys. Rev. Lett. **58**, 86 (1987).
[28] M. E. J. Newman and G. T. Barkema, *Monte Carlo Methods in Statistical Physics* (Clarendon, Oxford, 1999).

[29] D. P. Landau and K. Binder, *Monte Carlo Simulations in Statistical Physics* (Cambridge University Press, Cambridge, 2000).
[30] M. Weigel, Phys. Proc. **3**, 1499 (2010).
[31] J. Hoshen and R. Kopelman, Phys. Rev. B **14**, 3438 (1976).
[32] M. D'Onorio De Meo, D. Heermann, and K. Binder, J. Stat. Phys. **60**, 585 (1990).
[33] P. W. Kasteleyn and C. M. Fortuin, J. Phys. Soc. Jpn. **26**, 11 (1969); C. M. Fortuin and P. W. Kasteleyn, Physica **57**, 536 (1972); C. M. Fortuin, *ibid*. **58**, 393 (1972); **59**, 545 (1972).
[34] C.-K. Hu, Physica A **119**, 609 (1983); Phys. Rev. B **29**, 5103 (1984).
[35] T. W. Burkhardt and B. Derrida, Phys. Rev. B **32**, 7273 (1985).
[36] H. Watanabe, S. Yukawa, N. Ito, and C.-K. Hu, Phys. Rev. Lett. **93**, 190601 (2004).
[37] A. D. Bruce, J. Phys. C **14**, 3667 (1981).
[38] M. M. Tsypin and H. W. J. Blöte, Phys. Rev. E **62**, 73 (2000).
[39] A. Malakis and N. G. Fytas, Phys. Rev. E **73**, 056114 (2006).
[40] P. H. L. Martins and J. A. Plascak, Phys. Rev. E **76**, 012102 (2007).
[41] R. M. Ziff, Phys. Rev. Lett. **69**, 2670 (1992).
[42] C.-Y. Lin and C.-K. Hu, Phys. Rev. E **58**, 1521 (1998).
[43] J. L. Cardy, J. Phys. A **25**, L201 (1992).
[44] D. Stauffer and A. Aharony, *Introduction to Percolation Theory* (Taylor and Francis, London, 1994).
[45] J.-P. Hovi and A. Aharony, Phys. Rev. Lett. **76**, 3874 (1996).
[46] C.-K. Hu, Phys. Rev. B **29**, 5109 (1984).
[47] J. A. Plascak and P. H. L. Martins, Comput. Phys. Commun. **184**, 259 (2013).